OptIC Notch reveals mechanism that regulates receptor interactions with CSL.

Jonathan M. Townson, Maria J. Gomez-Lamarca, Sarah J. Bray*

Department of Physiology Development and Neuroscience,

University of Cambridge

Downing Street, Cambridge, CB2 3DY

*corresponding author: sjb32@cam.ac.uk

Key words: Notch, CSL, optogenetics, Drosophila, nuclear translocation.

Summary:

Active Notch signalling is brought about through receptor-ligand interactions that result in the release of the Notch intracellular domain (NICD) which translocates to the nucleus. NICD activates transcription at target sites in a tripartite complex with the DNA binding transcription factor CSL (CBF1/Su(H)/Lag-1) and co-activator Mastermind. Despite this, CSL lacks its own nuclear localisation sequence, and it remains unclear when and how the tripartite complex is formed. To probe the mechanisms involved, we designed an optogenetic approach to control NICD release (OptIC-Notch) and monitor consequences on complex formation and target gene activation. Strikingly we observed that, when uncleaved, OptIC-Notch sequesters CSL in the cytoplasm. Hypothesising that exposure of a juxta membrane ΦWΦP motif is key to sequestration, we masked this motif with a second light sensitive domain in OptIC-Notch{ω}, which was sufficient to prevent CSL sequestration. Furthermore, NICD produced by light induced cleavage of OptIC-Notch or OptIC-Notch{ω} chaperoned CSL into the nucleus and induced target gene activity, showing efficient light controlled Notch activation. Our results demonstrate that exposure of the ΦWΦP motif leads to recruitment of CSL and suggests that this is an important regulatory step in Notch signalling that can occur in the cytoplasm prior to nuclear entry.

Results and Discussion

Although predominantly nuclear in most cell-types examined, CSL does not contain a recognizable nuclear localization signal and it likely requires other factors to chaperone it into the nucleus. In overexpression experiments, NICD and several co-repressors, such as Hairless and SMRT, can fulfil this role and promote nuclear accumulation of CSL (Fortini and Artavanis-Tsakonas, 1994; Gho et al., 1996; Gomez-Lamarca et al., 2018; Maier, 2020; Tabaja et al., 2017; Wacker et al., 2011; Wolf et al., 2019, 2021; Zhou and Hayward, 2001). Although it has been widely assumed that NICD first meets CSL in the nucleus, there is no direct evidence to support this and it remains unclear whether the two proteins could interact prior to nuclear entry. The main argument against it is that CSL does not interact with the full-length transmembrane Notch receptor, despite the fact that NICD would be exposed in the cytoplasm. To investigate the relationship between NICD release and CSL transport into the nucleus, we developed OptIC-Notch, an optogenetic tool in which NICD is tethered to the membrane and released upon light activation.

Membrane tethered NICD can sequester CSL away from the nucleus.

OptIC-Notch uses the BLITz approach (Lee et al., 2017) in which light exposure simultaneously reconstitutes a TEV protease and reveals a TEV target site in the membrane tethered protein of interest, resulting in its release. In this case we used two constructs. In the first, a CIBN domain, N-terminal TEV protease fragment and a TEV cleavage-site motif were inserted between NICD tagged with mCherry and a heterologous transmembrane domain (CIBN-TEVn-mCherry-NICD, Fig. 1A). In the second, a cytoplasmic Cryptochrome 2 photolyase homology region was fused to a C-terminal TEV protease fragment (CRY-TEVc). When co-expressed, the active TEV protease will be reconstituted by light induced association of the CIBN and CRY domains, and can then cleave at its adjacent cleavage motif to release NICD fused to mCherry. As in the original BLITz, the TEV motif is protected by a light sensitive AsLOV2 domain (LOV) to prevent leaky cleavage (Fig. 1A). Expressing the trans-membrane construct in isolation will not support cleavage. We refer to this uncleavable condition as OptI-Notch and to the cleavable combination as OptIC-Notch.

Transgenic flies were generated to produce OptI-Notch and OptIC-Notch under the control of tissue-specific UAS-Gal4 combinations.

When expressed in *Drosophila* third instar larval salivary glands in the dark, OptIC-Notch was present in membranous structures throughout the cytoplasm and absent from the nucleus. Exposure to blue light resulted in rapid nuclear accumulation of cleaved NICD (Fig. 1B and 1C, Supp movie 1). Consistent with the dependence on blue light induced cleavage, the accumulation was weaker with longer wavelengths, that would be less effective at reconstituting TEV (496nm) and was non-existent in dark control conditions, where the salivary glands were not exposed to blue light (Fig. 1D). These results confirm that NICD can be released from OptIC-Notch in a light dependent manner.

To investigate the interactions between NICD and CSL, we expressed OptI-Notch/OptIC-Notch in the context of fluorescently tagged CSL (eGFP::CSL or Halo::CSL) present at endogenous levels (Gomez-Lamarca et al., 2018). Strikingly, in tissues expressing OptI-Notch, eGFP::CSL was strongly enriched in the cytoplasm with little or none present in the nucleus (Fig. 1E and F). In the cytoplasm, CSL colocalized with the OptI-Notch suggesting that it was becoming sequestered by interacting with the membrane tethered NICD. To confirm that CSL sequestration was mediated by its interaction with NICD, we performed the same experiment with a mutated version of CSL that is defective in Notch-binding (CSL[NBM] (Gomez-Lamarca et al., 2018; Yuan et al., 2016)). CSL[NBM] remained localised to the nucleus in the presence of OptI-Notch (1E and G). These data argue that CSL is sequestered by an interaction with the NICD moiety in OptI-Notch. Consistent with this hypothesis a different transmembrane tethered NICD, in which mCherry-NICD was fused to a CD8 transmembrane domain, also led to an abnormal CSL localization, with a significant fraction sequestered in the cytoplasm (Sup Fig. S1).

Released NICD chaperones CSL into the nucleus

Next, we investigated whether sequestered CSL could be effectively transported into the nucleus when NICD was released from the membrane. To test this possibility, larvae expressing OptIC-Notch were incubated in blue light for 24 hours. Under these conditions there was a clear change in CSL localisation, with a significant fraction relocating to the

nucleus (Fig. 2A, B and C). These results suggest that, having interacted with the membrane tethered NICD in the cytoplasm, CSL can be carried into the nucleus by NICD when it is released.

To rule out the possibility that the nuclear CSL is newly translated protein, which enters the nucleus independently and becomes stabilised by the released NICD, rather than previously sequestered CSL, we performed a pulsed labelling with the Halo ligand JF646. Salivary glands expressing Halo-CSL and OptIC-Notch were incubated with JF646 and subsequently washed to remove unbound ligand. Any CSL synthesized subsequently would thus be unlabelled. Cleavage of OptIC-Notch was then induced by blue light exposure whilst at the same time imaging JF646 bound Halo::CSL with far-red illumination. After two hours a clear nuclear accumulation of CSL was detected (Fig. 2D-F). The nuclear levels of NICD (Fig. 2G) and Halo::CSL (Fig. 2H) increased over time and the latter were proportional to the amount of nuclear NICD detected (Fig. 2I). Thus, the nuclear CSL corresponds to protein that was previously sequestered in the cytoplasm and that was likely transported to the nucleus by the released NICD.

We next asked whether NICD that is released by γ-secretase cleavage is also capable of transporting CSL into the nucleus. Because the co-repressor Hairless has an important role in transporting and stabilising CSL in the nucleus, we first used RNAi to knock down the expression of Hairless protein to avoid confounding effects. These conditions resulted in a decrease in the overall levels of nuclear CSL (Sup Fig. S2 A,B), as described previously (Gomez-Lamarca et al., 2018; Praxenthaler et al., 2017). When combined with a transgene producing constitutively cleaved Notch (Nact), the levels of nuclear CSL were largely restored, suggesting that released NICD is able to transport CSL into the nucleus (Sup Fig. S2C,D,E; and see (Gomez-Lamarca et al., 2018; Praxenthaler et al., 2017)). Altogether, the results demonstrate that CSL and NICD can interact in the cytoplasm and are co-transported into the nucleus. However, if this is indeed the case, it raises the question why CSL does not normally interact with the full-length endogenous Notch receptor before its cleavage (Gho et al., 1996).

Masking ΦWΦP motif prevents CSL interaction

One hypothesis to explain why CSL is sequestered by OptIC-Notch but not by the endogenous receptor, is that the high affinity CSL-binding ΦWΦP motif (Fig. 3A; Hall and Kovall, 2019) is exposed in OptIC-Notch but is normally hidden. It has been proposed that, in its normal context, this hydrophobic motif, which is located close to the transmembrane domain, becomes embedded in the lipid bilayer of the plasma membrane (Deatherage et al., 2017). This would occlude it from CSL until NICD is released from the membrane by γ-secretase cleavage. The insertion of several domains between the membrane and the ΦWΦP motif in OptIC-Notch could change the protein conformation, preventing the association of the motif with the membrane and making it available for binding with CSL.

If this hypothesis is correct, CSL should no longer be recruited by OptIC-Notch when the ΦWΦP motif is masked. To achieve this, we added a second LOV domain to the OptIC-Notch, six residues upstream of the ΦWΦP motif in NICD, here referred to as OptIC-Notch{ω} (Fig. 3B). In the dark, the additional LOV domain in OptIC-Notch{ω} will conceal the ΦWΦP motif. If this motif is responsible for the interaction, CSL should no longer interact with the NICD that is tethered to the membrane. Upon blue light activation the OptIC-Notch{ω} is cleaved in the same way as OptIC-Notch and, at the same time, the LOV domain concealing the ΦWΦP motif will unfold to make this motif available for CSL binding (Fig. 3B and 3C).

To assess the effects on CSL, we first expressed the membrane bound construct without the cytoplasmic CRY-TEVc (OptI-Notch{ω}). When kept in the dark, so that the ΦWΦP motif was protected by the LOV domain, CSL was no longer sequestered as predicted if the accessibility of the motif is a critical factor (Fig. 3D). Indeed, under these conditions the majority of CSL was detected in the nucleus with little retained in the cytoplasm in contrast to its localization with OptI-Notch (Fig. 3E). Furthermore, expression of OptI-Notch{ω} in the developing wing produced no discernible phenotype, unlike expression of the parent OptI-Notch which resulted in malformed adult wings with blisters and aberrant vein patterning likely due to reduced availability of CSL for endogenous Notch signalling (Sup Fig. S3).

Exposure of OptI-Notch{ω} to light should unmask the ΦWΦP motif, by unfolding the LOV domain, and, in the absence of CRY-TEVc, NICD will be tethered because no cleavage would occur. In these conditions a significant fraction of CSL became sequestered with the OptI-Notch{ω} outside the nucleus, consistent with the exposure of the ΦWΦP motif being a critical factor in its relocalization (3F and G). The sequestration was not as robust as that with the parent construct, because some CSL remained in the nucleus. Likely explanations are that a fraction of the CSL was retained there by interactions with nuclear proteins such as Hairless and/or that the unmasking was not 100% effective. Nevertheless, the fact that masking of the ΦWΦP motif largely eliminates CSL sequestration, and its unmasking partially reverses that, argues that this motif is responsible for the interaction. Furthermore, it is evident that the motif must be hidden in the native conformation of the endogenous receptor to prevent CSL sequestration and that its exposure upon cleavage is likely to be a key feature for promoting formation of the CSL-NICD transcription complex.

Light induced NICD release mimics Notch signalling

A final question is whether the light induced release of NICD from the membrane is competent to activate Notch signalling. As with OptIC-Notch, blue light activation of OptIC-Notch{ω} resulted in a rapid nuclear accumulation of NICD, indicative of efficient cleavage (Fig. 4A-C and 3C, MOV2). This did not occur with longer wavelengths of light that cannot induce the reconstitution of the TEV, confirming the specificity. Indeed, two hours of light were sufficient to bring about robust nuclear enrichment of NICD (Fig. 4B and C) and to promote the recruitment of CSL to the target *E(spl)-C* locus (Fig. 4D, E and F). This was visualized by the presence of an enriched band of CSL that co-localized with the fluorescent ParB-Int labelled genomic *E(spl)-C* locus, as described previously (Fig. 4E,F; (Gomez-Lamarca et al., 2018). Furthermore, robust expression of the Notch target gene *E(spl)mβ* was detected in blue light conditions, demonstrating that the released NICD was functional and able to induce target gene transcription (Fig 4G, 4H and 4I).

Conclusion:

In conclusion, our optogenetic tools to control release of NICD have revealed the importance of masking the ΦWΦP motif to prevent sequestration of CSL by the transmembrane receptor. When this motif is exposed, CSL interacts with NICD in the

cytoplasm. In our artificial constructs, the masking is achieved with a light-regulated LOV domain. In the native receptor it likely relies on shielding by association with membrane phospholipids (Deatherage et al., 2017). Tight regulation of domain-motif interactions is of fundamental importance for many central cellular processes, and frequently relies on post-translational modifications (Akiva et al., 2012). The membrane masking of the CSL binding motif in Notch is a novel example of such regulation. Furthermore, as CSL lacks a nuclear localisation motif, it raises the possibility that CSL partners with NICD in the cytoplasm once cleavage releases NICD from the membrane exposing the ΦWΦP motif. In this way, CSL would be transported into the nucleus with NICD after forming a complex in the cytoplasm.

Transportation between the nucleus and cytoplasm of transcription factors is one mechanism by which gene expression can be regulated in cell signalling (Cartwright and Helin, 2000; Fu et al., 2018; Di Ventura and Kuhlman, 2016; Xu and Massagué, 2004). Our results that CSL can be imported into the nucleus by NICD after first meeting in the cytoplasm imply nuclear import of CSL as one facet of the core regulatory mechanism in Notch signalling. It has also been observed that co-repressor binding to CSL can import or shuttle CSL in/out the nucleus (Tabaja et al., 2017; Wacker et al., 2011; Wolf et al., 2019; Zhou and Hayward, 2001). This raises the possibility that fine tuning the nuclear import of activator and repressor complexes will have an important role in determining whether the activation complex “wins out” for binding to CSL target sites to turn on their expression.

Cleavage of OptIC-Notch{ω} is sufficient to translocate CSL into the nucleus and to promote transcription in less than 2 hours. This timeframe is similar to that seen with other approaches for ligand independent Notch activation (Falo-Sanjuan and Bray, 2020) and demonstrates the potential of using light controlled activation to probe mechanisms required for generating rapid transcriptional responses.

Acknowledgements

We thank Kat Millen and The University of Cambridge Department of Genetics Fly Facility for performing DNA injections of fly embryos to generate transgenic stocks. We are grateful to Cambridge Advanced Imaging Centre, and all members of the Bray Lab, for helpful discussions. We also acknowledge Servier Medical Art, provided by Servier, for images used in the generation of figures 1A and 3B. The work was funded by a Wellcome Trust Investigator Award to SJB (212207/Z/18). JT was supported by a G.H.Lewes/BBSRC studentship (1944853). For the purpose of open access, the author has applied a Creative Commons Attribution (CC BY) licence to any Author Accepted Manuscript version arising from this submission.

Author contributions.

JT, MGL and SJB designed the experiments. JT performed the experiments. MGL generated critical reagents. JT and SJB analysed the data. JT and SJB wrote the manuscript, MGL reviewed and commented on the manuscript.

Declaration of interests

The authors declare that they have no competing interests.

References cited

Akiva, E., Friedlander, G., Itzhaki, Z., and Margalit, H. (2012). A dynamic view of domain-motif interactions. PLoS Comput. Biol. *8*.

Bischof, J., Maeda, R.K., Hediger, M., Karch, F., and Basler, K. (2007). An optimized transgenesis system for Drosophila using germ-line-specific ϕC31 integrases. Proc. Natl. Acad. Sci. U. S. A. *104*, 3312–3317.

Boukhatmi, H., and Bray, S. (2018). A population of adult satellite-like cells in Drosophila is maintained through a switch in RNA-isoforms. Elife *7*, 1–24.

Cartwright, P., and Helin, K. (2000). Nucleocytoplasmic shuttling of transcription factors. Cell. Mol. Life Sci. *57*, 1193–1206.

Cruz, C., Glavic, A., Casado, M., and De Celis, J.F. (2009). A gain-of-function screen identifying genes required for growth and pattern formation of the Drosophila melanogaster wing. Genetics *183*, 1005–1026.

Deatherage, C.L., Lu, Z., Kroncke, B.M., Ma, S., Smith, J.A., Voehler, M.W., McFeeters, R.L., and Sanders, C.R. (2017). Structural and biochemical differences between the Notch and the amyloid precursor protein transmembrane domains. Sci. Adv. *3*.

Falo-Sanjuan, J., and Bray, S.J. (2020). Decoding the Notch signal. Dev. Growth Differ. *62*, 4–14.

Fortini, M.E., and Artavanis-Tsakonas, S. (1994). The Suppressor of Hairless Protein Participates in Notch Receptor Signaling. Cell *79*, 273–282.

Fortini, M.E., Rebay, I., Caron, L.A., and Artavanis-Tsakonas, S. (1993). An activated Notch receptor blocks cell-fate commitment in the developing Drosophila eye. Nature *365*, 555–557.

Fu, X., Liang, C., Li, F., Wang, L., Wu, X., Lu, A., Xiao, G., and Zhang, G. (2018). The rules and functions of nucleocytoplasmic shuttling proteins. Int. J. Mol. Sci. *19*, 1–17.

Gho, M., Lecourtois, M., Géraud, G., Posakony, J.W., and Schweisguth, F. (1996). Subcellular localization of suppressor of hairless in Drosophila sense organ cells during Notch signalling. Development *122*, 1673–1682.

Gomez-Lamarca, M.J., Falo-Sanjuan, J., Stojnic, R., Abdul Rehman, S., Muresan, L., Jones, M.L., Pillidge, Z., Cerda-Moya, G., Yuan, Z., Baloul, S., et al. (2018). Activation of the Notch Signaling Pathway In Vivo Elicits Changes in CSL Nuclear Dynamics. Dev. Cell *44*, 611–

623.

Grusch, M., Schelch, K., Riedler, R., Reichhart, E., Differ, C., Berger, W., Inglés-Prieto, Á., and Janovjak, H. (2014). Spatio-temporally precise activation of engineered receptor tyrosine kinases by light. EMBO J. *33*, 1713–1726.

Hall, D.P., and Kovall, R.A. (2019). Structurally conserved binding motifs of transcriptional regulators to notch nuclear effector CSL. Exp. Biol. Med. *244*, 1520–1529.

Krejčí, A., and Bray, S. (2007). Notch activation stimulates transient and selective binding of Su(H)/CSL to target enhancers. Genes Dev. *21*, 1322–1327.

Lee, D., Creed, M., Jung, K., Stefanelli, T., Wendler, D.J., Oh, W.C., Mignocchi, N.L., Lüscher, C., and Kwon, H.B. (2017). Temporally precise labeling and control of neuromodulatory circuits in the mammalian brain. Nat. Methods *14*, 495–503.

Maier, D. (2020). Membrane-anchored hairless protein restrains notch signaling activity. Genes (Basel). *11*, 1–23.

Praxenthaler, H., Nagel, A.C., Schulz, A., Zimmermann, M., Meier, M., Schmid, H., Preiss, A., and Maier, D. (2017). Hairless-binding deficient Suppressor of Hairless alleles reveal Su(H) protein levels are dependent on complex formation with Hairless. PLoS Genet. *13*, 1–23.

Rebay, I., Fehon, R.G., and Artavanis-Tsakonas, S. (1993). Specific truncations of Drosophila Notch define dominant activated and dominant negative forms of the receptor. Cell *74*, 319–329.

Roy, S., and VijayRaghavan, K. (1997). Homeotic genes and the regulation of myoblast migration, fusion, and fibre-specific gene expression during adult myogenesis in Drosophila. Development *124*, 3333–3341.

RStudio Team (2020). RStudio: Integrated Development for R.

Schneider, C.A., Rasband, W.S., and Eliceiri, K.W. (2012). NIH Image to ImageJ: 25 years of image analysis. Nat. Methods *9*, 671–675.

Tabaja, N., Yuan, Z., Oswald, F., and Kovall, R.A. (2017). Structure-function analysis of RBP-J-interacting and tubulin-associated (RITA) reveals regions critical for repression of Notch target genes. J. Biol. Chem. *292*, 10549–10563.

Di Ventura, B., and Kuhlman, B. (2016). Go in! Go out! Inducible control of nuclear localization. Curr. Opin. Chem. Biol. *34*, 62–71.

Wacker, S.A., Wichert, V., Clau, K., Nienhaus, G.U., Hameister, H., Baumann, B., and

Oswald, F. (2011). RITA , a novel modulator of Notch signalling , acts via nuclear export of RBP-J. EMBO J. *30*, 43–56.

Wolf, D., Smylla, T.K., Reichmuth, J., Hoffmeister, P., Kober, L., Zimmermann, M., Turkiewicz, A., Borggrefe, T., Nagel, A.C., Oswald, F., et al. (2019). Nucleo-cytoplasmic shuttling of Drosophila Hairless/Su(H) heterodimer as a means of regulating Notch dependent transcription. Biochim. Biophys. Acta - Mol. Cell Res. *1866*, 1520–1532.

Wolf, D.B., Maier, D., and Nagel, A.C. (2021). Nucleo-cytoplasmic shuttling of murine RBPJ by Hairless protein matches that of Su(H) protein in the model system Drosophila melanogaster. Hereditas *158*, 1–6.

Xu, L., and Massagué, J. (2004). Nucleocytoplasmic shuttling of signal transducers. Nat. Rev. Mol. Cell Biol. *5*, 209–219.

Yuan, Z., Praxenthaler, H., Tabaja, N., Torella, R., Preiss, A., Maier, D., and Kovall, R.A. (2016). Structure and Function of the Su(H)-Hairless Repressor Complex, the Major Antagonist of Notch Signaling in Drosophila melanogaster. PLoS Biol. *14*, 1–26.

Zhou, S., and Hayward, S.D. (2001). Nuclear Localization of CBF1 Is Regulated by Interactions with the SMRT Corepressor Complex. Mol. Cell. Biol. *21*, 6222–6232.

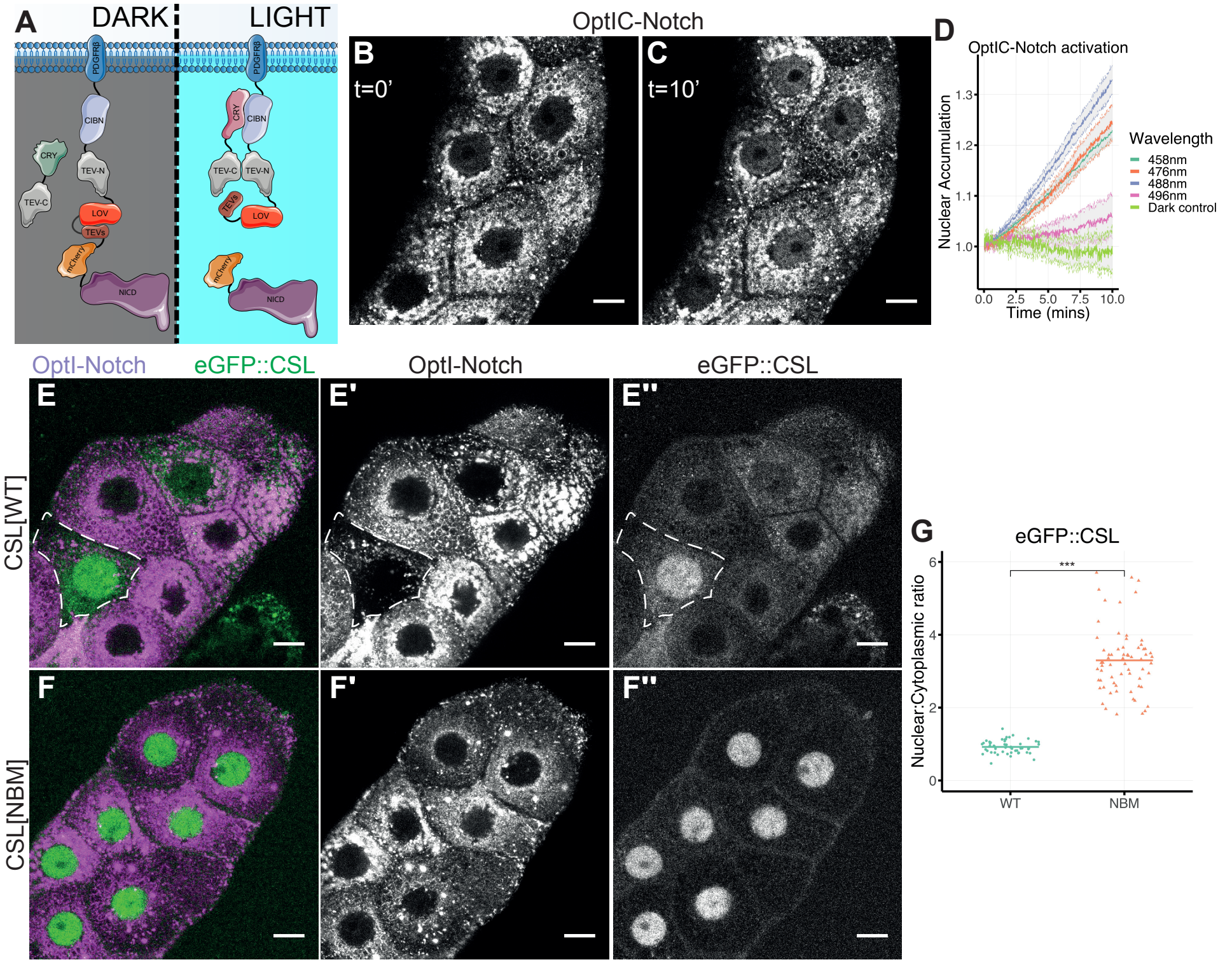

Figure 1: CSL is sequestered away from the nucleus by OptIC-Notch through interaction with NICD.
(A) Schematic depicting the domain structure of OptIC-Notch and the changes brought about by exposure to blue light to release NICD (purple). Blue light induces (i) heterodimerisation of CRY2 (green) and CIBN (lilac) domains, reconstituting TEV protease (TEV-C and TEV-N; grey) (ii) unfolding of LOV (Red) to reveal a TEV cleavage site (TEVs, Brown) which is cut by TEV, releasing NICD.
(B-C) Localization of OptIC-Notch in salivary glands before (B; t=0') and after 10 minutes exposure to 458nm (blue) light (C, t=10'); mCherry::NICD is detected in the nucleus when cleavage is induced by light exposure. Scale bar = 20 μm.
(D) Nuclear accumulation of mCherry::NICD after exposure of salivary glands expressing OptIC-Notch to different wavelengths of light over time. Dark controls were not exposed to light (mean ± SEM).
(E) Localisation of eGFP::CSL (green, E, single channel E'') in salivary glands cells expressing OptI-Notch (magenta, E, single channel E'; driven by 1151-Gal4 without CRY-TEVc). eGFP::CSL is detected outside the nucleus in most cells, dashed outline indicates a cell with low levels of OptI-Notch where eGFP::CSL remains nuclear. Scale bar = 20 μm.
(F) Notch binding mutant (NBM) variant of eGFP::CSL (green, F, single channel F'') is not sequestered by OptI-Notch (magenta, F, single channel F'), conditions as in E. Scale bar = 20 μm. (G) Nuclear to cytoplasmic ratio of eGFP::CSL[WT] and eGFP::CSL[NBM] in the presence of OptI-Notch (without CRY-TEVc). Bar represents the mean of ≥10 salivary glands per condition. Welch's t-test p-value < 0.001.

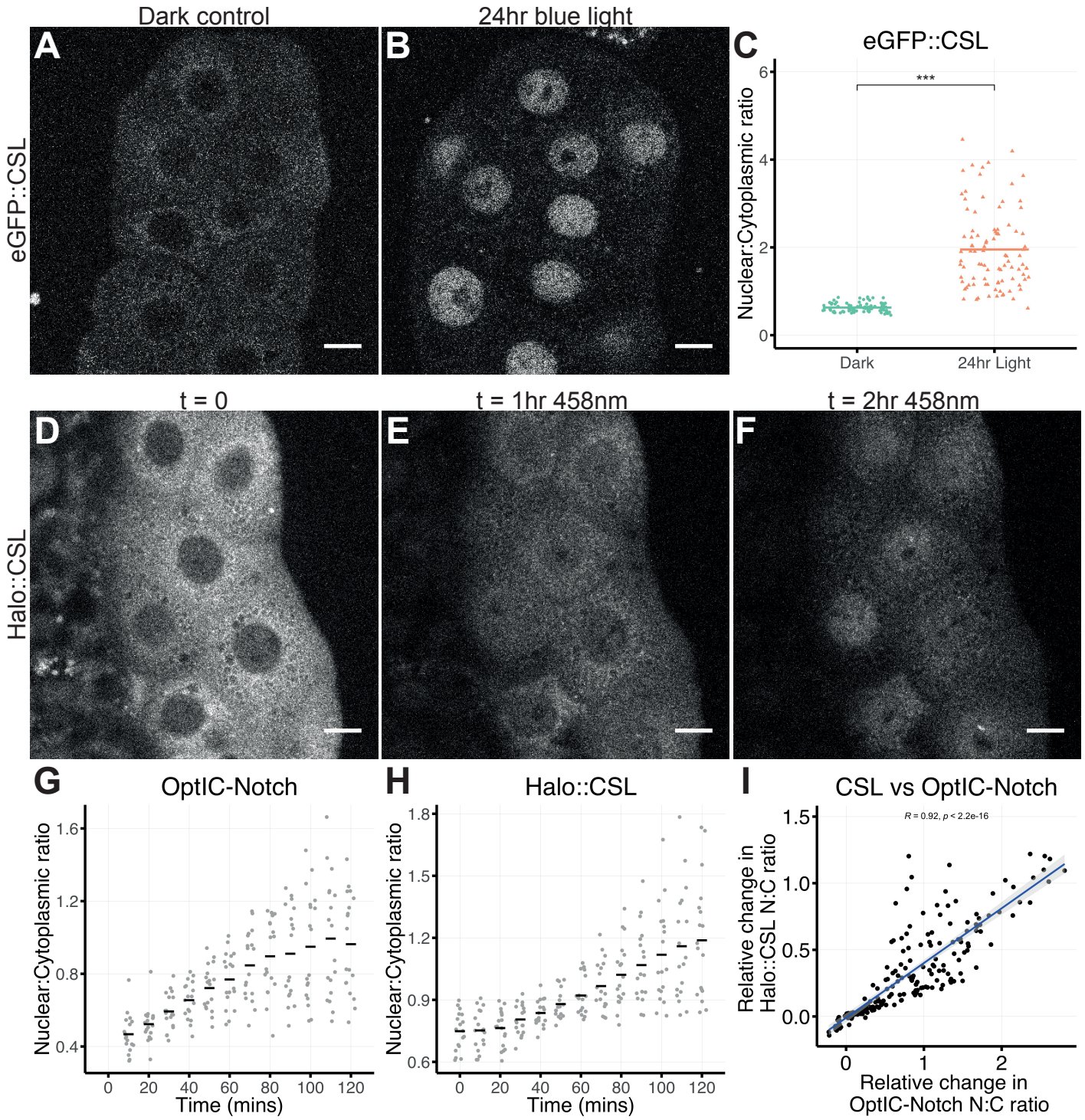

Figure 2: CSL relocalises to the nucleus when NICD is released

(A,B) Localisation of eGFP::CSL in salivary glands expressing OptIC-Notch without activation (A) and after 24hrs of blue light induced activation (B). Cytoplasmic sequestration of eGFP::CSL is reversed. Scale bar = 20 µm.

(C) Nuclear to cytoplasmic ratio of eGFP::CSL is significantly increased after 24 hours of activation Bar represents the mean of >10 salivary glands per condition. Welch's t-test p-value < 0.001.

(D-F) Localization of Halo::CSL in the presence of OptIC-Notch detected before (t=0) and after exposure to continuous blue light (458 nm) for the indicated times. Salivary glands were exposed to JF646 to label Halo::CSL prior to imaging. By 2hrs a significant fraction of Halo::CSL has translocated to the nucleus. Scale bar = 20 µm.

(G-H) Light exposure leads to increased nuclear:cytoplasmic ratio of OptIC-Notch (G, indicative of cleavage to release GFP::NICD) and of Halo::CSL (H).

(I) Rate of nuclear accumulation of GFP::NICD and of Halo::CSL. The two are correlated (Spearmans test, Rho=0.92, p < 0.001).

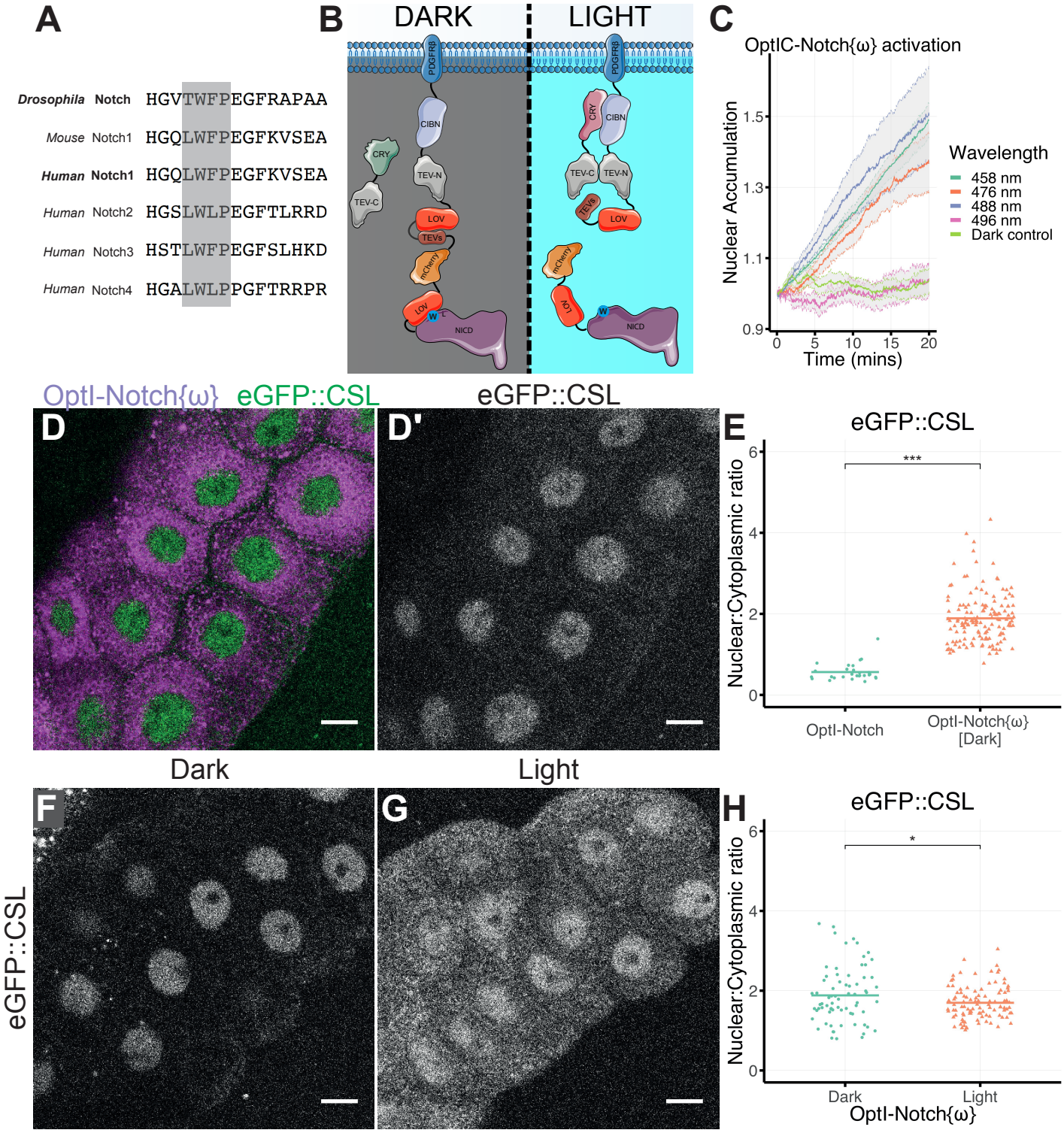

Figure 3: Masking ΦWΦP motif prevents sequestration

(A) Sequence alignment of residues at the N-terminus of NICD from the indicated Notch receptors shows strong conservation of the ΦWΦP motif (grey shading).

(B) Schematic showing the modified optogenetic construct, OptIC-Notch{ω}, containing an additional LOV domain (red) to mask the ΦWΦP motif (blue, W) in NICD. Other domains are as in Fig. 1A.

(C) Nuclear accumulation of mCherry::NICD after exposure of salivary glands expressing OptIC-Notch{ω} to different wavelengths of light over time. Dark controls were not exposed to light (mean ± SEM).

(D) eGFP::CSL (D, green; D') is nuclear in the presence of OptI-Notch{ω} without CRY-TEVc (D, magenta).

(E) Nuclear to cytoplasmic ratio of eGFP::CSL in tissues expressing OptI-Notch{ω} in comparison to OptI-Notch (both without CRY-TEVc). Significantly higher ratios are detected with OptI-Notch{ω}. Bar represents the mean of ≥5 salivary glands per condition. Welch's t-test p-value < 0.001.

(F-H) Nuclear localization of eGFP::CSL in tissues expressing OptI-Notch{ω} (without CRY-TEVc) (F) is altered upon light exposure to a more even cellular distribution (G) and overall the nuclear to cytoplasmic ratio is reduced (H). In (H) Bar represents the mean of > 10 salivary glands per condition. Welch's t-test p-value = 0.048. Scale bars in D,F,G = 20 µm.

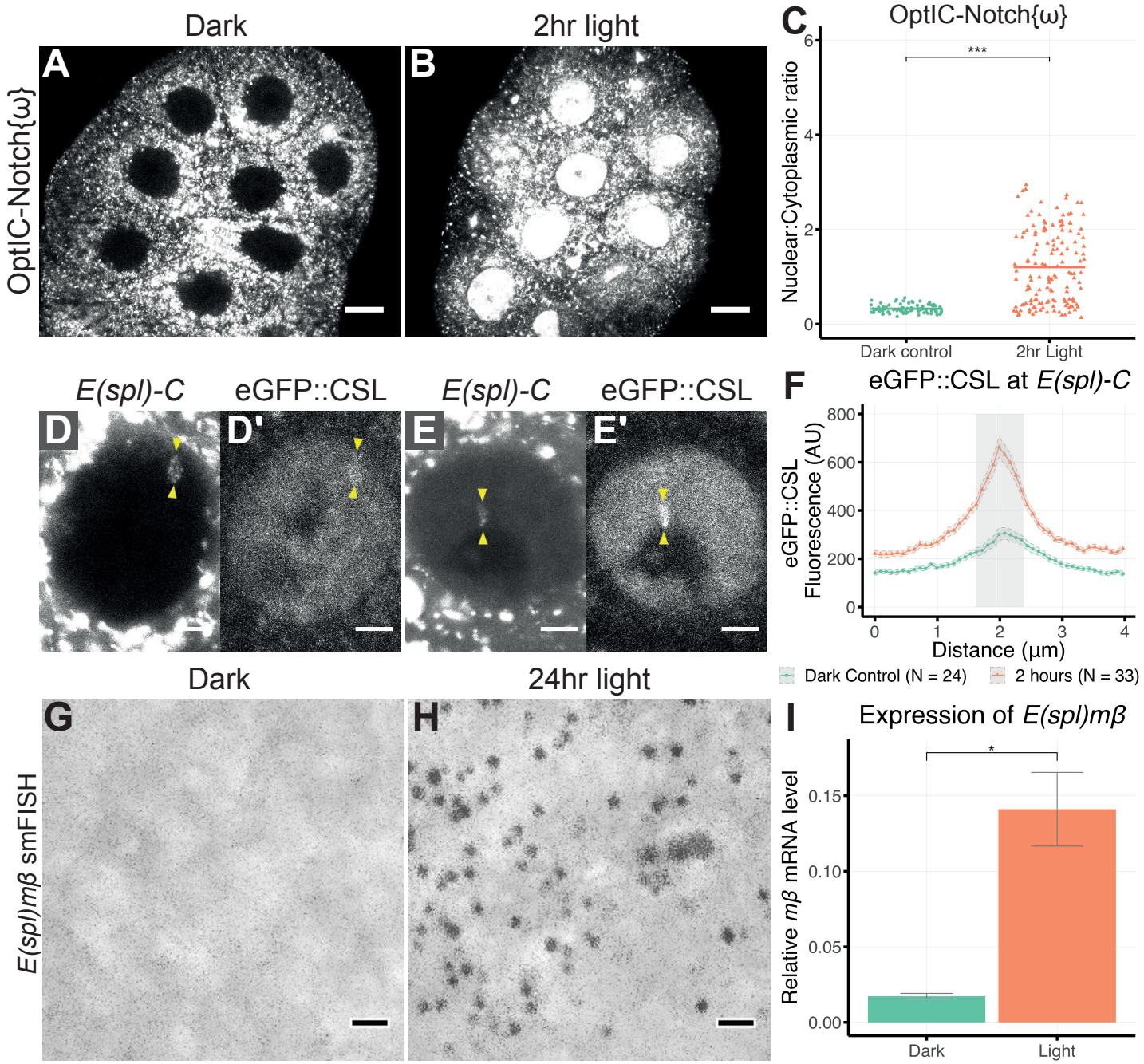

Figure 4: Light induced cleavage of OptIC-Notch{ω} relocates CSL and promotes transcription
(A-B) Localization of OptIC-Notch{ω} before (A) and after 2hrs blue light (B). Strong nuclear localisation of mCherry::NICD in B is indicative of efficient light induced cleavage.
(C) Nuclear to cytoplasmic ratio of mCherry in salivary glands kept in the dark and 2hrs light. Bar represents the mean of >10 salivary glands. Welch's T-test p value < 0.001.
(D-F) Nuclear distribution of eGFP::CSL in the presence of OptIC-Notch{ω}. No/little enrichment at *E(spl)-C* is detected in dark conditions (D',F), strong enrichment at the *E(spl)-C* locus is detected within 2hrs of light (E',F). *E(spl)-C* is detected using the parB-Int system in D, E, the corresponding region is depicted by grey shading in F, eGFP fluorescence intensity was quantified in relation to the tagged locus. Error bars = ± SEM.
(G-H) Detection of cytoplasmic *E(spl)mβ* transcripts (black spots), by single molecule fluorescence *in situ* hybridization (smFISH) from salivary glands kept in the dark (G) or after 24hr blue light (H), transcripts are shown overlaid on transmitted light, scale bar = 1µm. (I) Quantification of *E(spl)mβ* RNA by RT-qPCR in the two conditions shows significant increase, N=3, error bars are ± SEM. Welch's t-test p-value = 0.036.

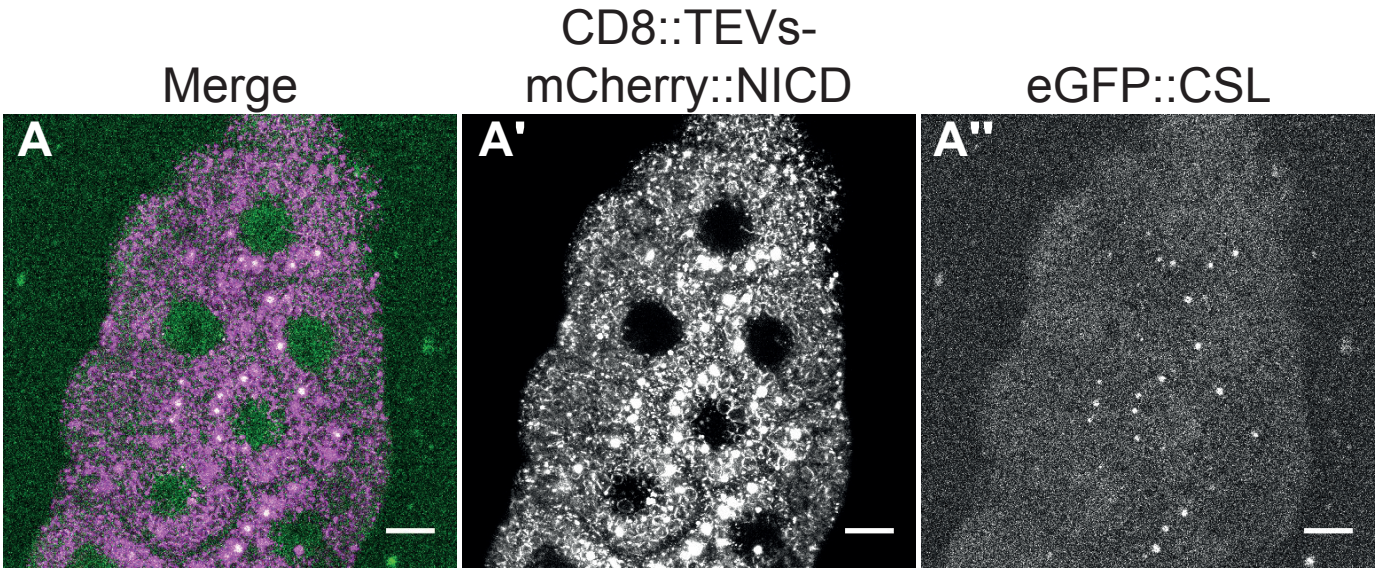

Supplementary Figure 1: CSL is sequestered by additional constructs containing NICD.
(A) Localisation of eGFP::CSL in salivary glands expressing (with 1151-Gal4) NICD bound to membranes via a CD8 moiety with a TEV sequence and mCherry tag in between (A'). CSL is partially sequestered in the cytoplasm (A''). Scale bar = 20 µm.

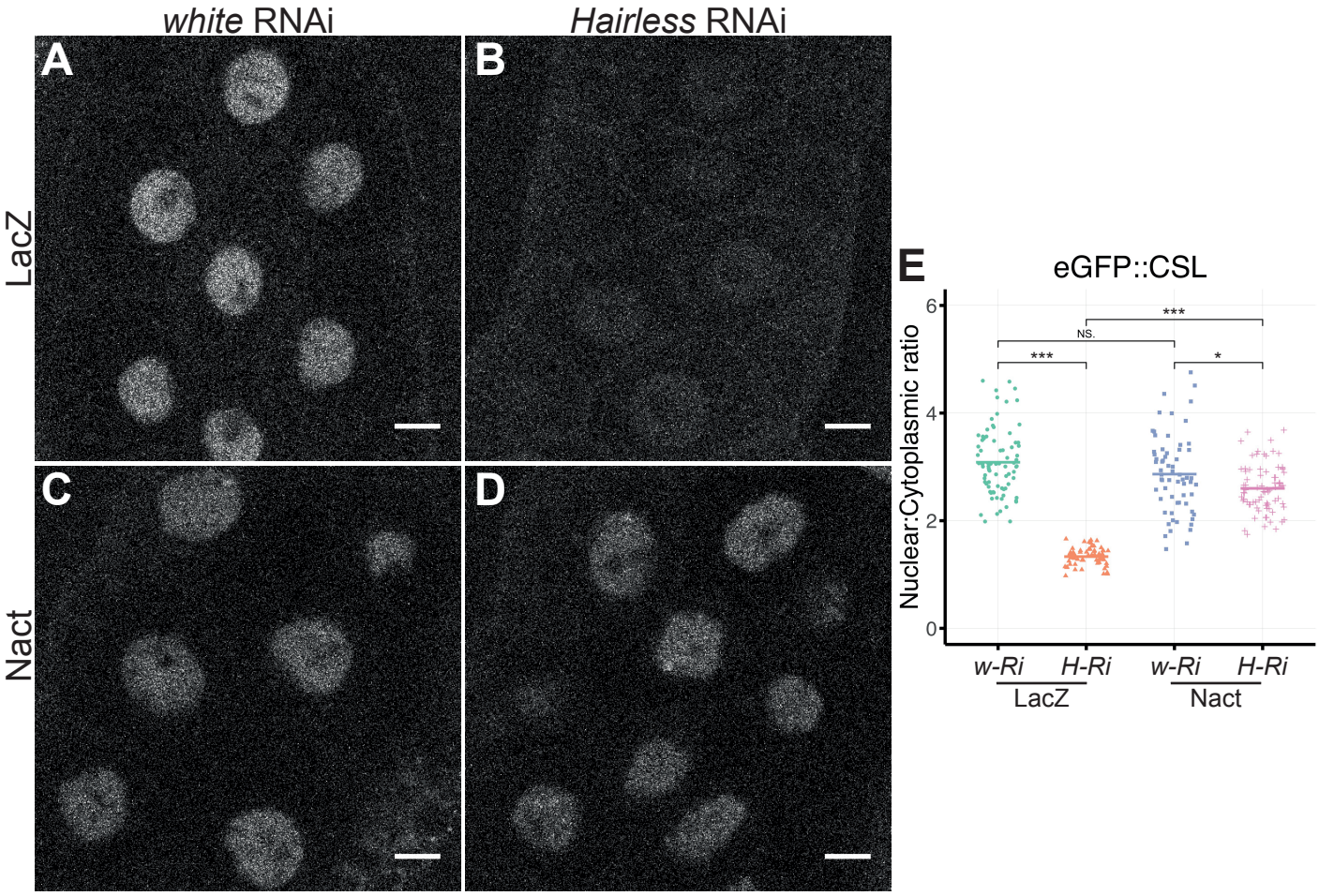

Supplementary Figure 2: Constitutively cleaved Notch is sufficient to return CSL to nucleus in the absence of Hairless.

(A-D) Localisation of eGFP::CSL in salivary glands expressing LacZ or Nact (the constitutively active Notch, NΔECD) with *white* RNAi (A, C) or *Hairless* RNAi (B, D). A large decrease in CSL levels is seen in the absence of Hairless (B) This decrease in CSL levels is not seen in the absence of Hairless (D). Scale bar = 20 μm.

(E) Nuclear to cytoplasmic ratio of eGFP::CSL in tissues expressing LacZ or Nact in a *white* or *Hairless* RNAi background. Bars represent the mean of >10 salivary glands per condition. Welch's t-test p-values for LacZ *w-Ri* vs *H-Ri* < 0.001, Nact *w-Ri* vs *H-Ri* = 0.012, *H-Ri* LacZ vs Nact < 0.001.

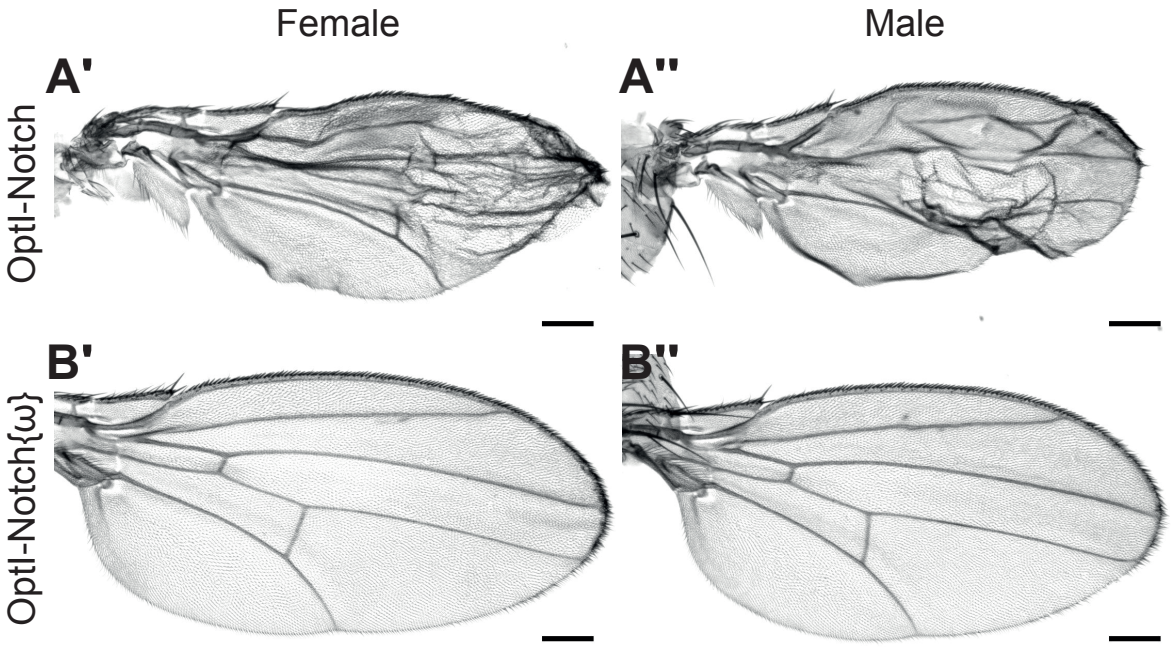

Supplementary Figure 3: OptI-Notch{ω} does not generate phenotypes in wings seen with OptI-Notch. Opti-Notch (A) or OptI-Notch{ω} (B) is expressed using SalpGal4 in the wing in both males and females. Blistering and aberrant vein patterning is seen with OptI-Notch and not OptI-Notch{ω}. Scale bar = 100 μm.

Supplementary Movie 1: Release of NICD from OptIC-Notch.

OptIC-Notch is activated with 458 nm light for 10 minutes. Release of NICD and its accumulation in the nucleus over time is shown by simultaneous imaging of the mCherry tag.

Supplementary Movie 2: Release of NICD from OptIC-Notch{ω}

OptIC-Notch{ω} is activated with 458 nm light for 20 minutes. Release of NICD and its accumulation in the nucleus over time is shown by simultaneous imaging of the mCherry tag.

STAR methods

RESOURCE AVAILABILITY

Lead contact

Further information and requests for resources and reagents should be directed to, and will be fulfilled by, the Lead Contact, Sarah J Bray (sjb32@cam.ac.uk).

Materials availability

All stocks, plasmids, and reagents generated in this study are available from the Lead Contact but we may require a completed Materials Transfer Agreement.

Data and code availability

Microscopy data reported in this paper will be shared by the lead contact upon request.

All original code has been deposited at Zenodo and is publicly available as of the date of publication. DOIs are listed in the key resources table.

Any additional information required to reanalyze the data reported in this paper is available from the lead contact upon request.

Key Resources Table

REAGENT or RESOURCE	SOURCE	IDENTIFIER
Chemicals, peptides, and recombinant proteins		
Shield and Sang M3 insect medium	Sigma Aldrich	Cat #: S3652
Fetal Bovine Serum	Sigma Aldrich	Cat #: F9665
Antibiotic-antimicotic	Gibco	Cat #: 15240062
Poly-L-lysine hydrobromide	Sigma Aldrich	Cat #: P9155
Methyl-cellulose	Sigma Aldrich	Cat #: M0387
Janelia Fluor® 646 HaloTag® Ligand	Promega	Cat #: GA112A
TRI reagent	Invitrogen	Cat #: AM9738
Oligo(dT) primers	Promega	Cat #: C1101
RiboLock RNase inhibitor	Thermo Scientific	Cat #: EO0381
M-MLV reverse transcriptase	Promega	Cat #: M1701
Stellaris RNA FISH Hybridization Buffer	Bioresearch Technologies	Cat #: SMF-HB1-10
Stellaris RNA FISH Wash Buffer A	Bioresearch Technologies	Cat #: SMF-WA1-60
Stellaris RNA FISH Wash Buffer B	Bioresearch Technologies	Cat #: SMF-WB1-20
Critical commercial assays		
Ambion's DNA-free DNA removal kit	Invitrogen	Cat #: AM1906
LightCycler 480 SYBR Green I Master PCR kit	Roche	Cat #: 04707516001
Experimental models: Organisms/strains		
D. melanogaster 1151-Gal4;;	Laboratory of Lingadahalli S. Shashidhara	Flybase:FBti0007229
D. melanogaster Salp-Gal4	(Cruz et al., 2009)	Flybase:FBtp0021755. RRID:BDSC_80573

D. melanogaster ;;UAS-*white*-RNAi	Bloomington Drosophila Stock Center	Flybase:FBti0144194. RRID:BDSC_35573
D. melanogaster ;;UAS-*Hairless*-RNAi	Bloomington Drosophila Stock Center	Flybase:FBst0027315. RRID:BDSC_27315
D. melanogaster ;UAS-NΔECD;	(Fortini et al., 1993; Rebay et al., 1993)	N/A
D. melanogaster ;;*E(spl)m8intA*,UAS-ParB1::mCherry	(Gomez-Lamarca et al., 2018)	N/A
D. melanogaster ;;eGFP::CSL	(Gomez-Lamarca et al., 2018)	N/A
D. melanogaster ;;eGFP::CSL[NBM]	(Gomez-Lamarca et al., 2018)	N/A
D. melanogaster ;;Halo::CSL	This paper	N/A
D. melanogaster ;UAS-CRYTEVc (AttP40);	This paper	N/A
D. melanogaster ;UAS-CRYTEVc (AttP51C);	This paper	N/A
D. melanogaster ;;UAS-OptIC-Notch[GFP] (AttP86Fb)	This paper	N/A
D. melanogaster ;;UAS-OptIC-Notch[mCherry] (AttP86Fb)	This paper	N/A
D. melanogaster ;;UAS-OptIC-Notch{ω}[mCherry] (AttP86Fb)	This paper	N/A
D. melanogaster ;UAS-OptIC-Notch{ω}[mCherry] (AttP40);	This paper	N/A
D. melanogaster ;UAS-OptIC-Notch{ω}[mCherry] (AttP40), UAS-CRYTEVc (AttP51C);	This paper	N/A
D. melanogaster ;;UAS-CD8_TEVs_mCherry_NICD (AttP86Fb)	This paper	N/A
Oligonucleotides		
Oligonucleotides for mRNA measurements	(Gomez-Lamarca et al., 2018)	Table S1
Recombinant DNA		
pCMV-NES-CRY2PHR-TevC	(Lee et al., 2017)	RRID:Addgene_89877
pCMV-TM-CIBN-BLITz1-TetR-VP16	(Lee et al., 2017)	RRID:Addgene_89878
Software and algorithms		
ImageJ	(Schneider et al., 2012)	https://imagej.net/ij/index.html
RStudio	(RStudio Team, 2020)	https://posit.co/
Other		
R Scripts	This paper	10.5281/zenodo.7607780
HerpNursery II	Lucky Reptile	Model #: CLH501 ASIN: B002NFR0HQ
LED strip lights of 300 5050 RGB LEDs	Nothing Fancy	ASIN: B07Q74XMTQ
Amber book light	LENCENT	ASIN: B082HCTY7W

EXPERIMENTAL MODEL AND SUBJECT DETAILS

Drosophila melanogaster strains and genetics

All *Drosophila melanogaster* stocks were grown on standard medium at 25 °C. Details of

stocks used are available in the key resources table. Expression from the indicated constructs was driven using *1151-Gal4* in the salivary glands and *Salp-Gal4* in wing discs (Cruz et al., 2009; Roy and VijayRaghavan, 1997).

For keeping larvae in the dark, vials were wrapped in aluminium foil and kept in a thick cardboard box. For global blue light illumination, a blue light incubator was built as in (Grusch et al., 2014). Briefly, an incubator with temperature control (LuckyReptile, HerpNursery II) was fitted with LED strip lights of 300 5050 RGB LEDs and set to constant blue illumination. Larvae were placed in the incubator on apple juice plates supplemented with yeast, for maximal light exposure, according to the length of time specified. For the inducible sequestration experiments larvae were grown in the light from embryos laid on apple juice plates and corresponding dark controls were grown the same way, wrapped in foil inside a cardboard box.

Generation of optogenetic fly lines and Halo::CSL

BLITz constructs (Lee et al., 2017) were obtained from Addgene (89877 and 89878) and the tTA domain replaced with an NICD fragment (residues T1766 to I2703 of the full-length *Drosophila* Notch receptor, Uniprot P07207), tagged with mCherry or GFP at the N terminus, by restriction digestion cloning to generate OptIC-Notch. The second LOV domain in OptIC-Notch{ω} was added by Gibson cloning between position R1768 and K1769 (numbering of the full-length Notch receptor) to the NICD fragment of OptIC-Notch. The CD8-TEVs-mCherry-NICD construct was cloned by the replacement of the BLITz element in OptIC-Notch with CD8-TEVs using restriction digest cloning. All constructs were then cloned into a UASt vector containing AttB integration sites (Bischof et al., 2007).

Transgenic optogenetic fly lines were generated by injection of plasmid DNA into embryos and integration by germ-line specific ΦC31 integrases (Bischof et al., 2007) into AttP sites on the second and third chromosome (AttP40, AttP51C, AttP86Fb). Male transgenics were selected using miniwhite.

A Halo::CSL construct expressed at endogenous levels was generated as in (Gomez-Lamarca et al., 2018), using a Halo tag in place of the N-terminal GFP tag. Labelling of the tag was

performed by keeping dissected salivary glands in dissection media containing 1 µM of JF646 ligand (Promega, GA112A) for 15 minutes, followed by three 15-minute washes in dissection media.

Sample dissection and mounting

Salivary glands were dissected from third instar larvae in M3 Shields and Sang media (Sigma, S3652) supplemented with 5% foetal bovine serum (Sigma, F9665) and 1x Antibiotic-Antimycotic (Gibco, 15240-062). For optogenetic experiments dissections were performed using only a red-light source (LENCENT) for illumination. Salivary glands were subsequently mounted on poly-lysine treated cover slips in dissection media supplemented with 2.5% methyl-cellulose (Sigma, M0387-100G) as in (Gomez-Lamarca et al., 2018).

Wings were dissected from adult flies three days after eclosion and mounted in glycerol. Images were captured using a Zeis Axioplan 2 microscope with a 5x air objective, Retiga EXi camera, and volocity 6.3.1 software.

METHOD DETAILS

Live imaging

Live confocal fluorescence imaging was performed on a Leica SP8 microscope equipped with an Argon laser and 561/633 nm He/Ne lasers using a 63x/1.4 NA HC PL APO CS2 oil immersion objective and two hybrid GaAsP detectors. Nuclei were imaged with an additional 4x zoom. For most experiments, Z-stacks were taken to cover the whole tissue with a step size of 1 µm, a resolution of 512x512px, pinhole set to 3-Airy, 12-bit depth and scanning at 400 Hz. For movies, a single plane was imaged every 2.58 seconds, using the same settings as with Z stacks. We use sequential scanning to acquire images of green fluorescent protein using 488 nm excitation or to provide activating blue light for optogenetics (typically 458nm), and either excitation wavelengths of 561 nm or 633 nm light for red and far-red fluorescence.

Quantitative RT-qPCR and *in situ* hybridizations

Single molecule fluorescent *in situ* hybridization was performed following the Stellaris protocol as in (Boukhatmi and Bray, 2018).

For RT-qPCR, phenol-chloroform extraction of RNA (using TRI reagent - Invitrogen, AM9738) was performed on 20 animals for each condition and precipitated at -20 °C overnight. Precipitated RNA was pelleted and washed with 70% ethanol, then resuspended in DEPC treated water. A DNAse reaction was perform on 5 µg of RNA (Invitrogen, AM1906) and 2 µg of RNA subsequently reverse transcribed into cDNA with MMLV Reverse Transcriptase and oligo-dT primers (Promega, M1701 and C110A). Quantitative PCR was performed using a Roche Lightcycler 480 II with SYBR green mastermix and primers (Sigma) targeted against the *E(spl)mβ* coding sequence (Gomez-Lamarca et al., 2018; Krejčí and Bray, 2007). Relative amounts of mRNA were then calculated normalised to the control gene *RpL32*. Two technical repeats of the qPCR were completed for each experiment and the mean taken for analysis, replicate numbers refer to the number of biological repeats where the full experimental protocol was completed from start to finish.

QUANTIFICATION AND STATISTICAL ANALYSIS

Image and statistical analysis

Image and video analysis was performed in ImageJ and RStudio (RStudio Team, 2020; Schneider et al., 2012).

For quantifying optogenetic movies and images, regions of interest were manually drawn around the whole cell and nucleus of each cell within a salivary gland. From this the mean nuclear and cytoplasmic fluorescence were calculated. Nuclear accumulation was measured as the mean nuclear fluorescence intensity at each timepoint divided by the initial measurement. The nuclear:cytoplasmic ratio is the mean nuclear fluorescence divided by the cytoplasmic fluorescence.

For quantifying recruitment of CSL to the *E(spl)-C* locus, images were rotated so the locus was a vertical line, a box of width 4 µm (45px) and height of the locus tag “band” was drawn and the “plot profile” function of ImageJ used to measure the increase fluorescence across the locus. We aligned all measurements such that the maximum locus tag signal was in the centre of the profile.

Table S1: List of Oligonucleotides. Related to STAR methods.

Name	**Sequence**
E(spl)mβ forward	GCTGGACTTGAAACCGC
E(spl)mβ reverse	AGAAGTGAGCAGCAGCC
RpL32 forward	ATGCTAAGCTGTCGCACAAATG
RpL32 reverse	GTTCGATCCGTAACCGATGT